21PM1E-03

A Radiation Assessment Apparatus Applicable to mmWave Antennas based on a 2D Scanner

Yun-Tsung Tu[#1], Wen-Jiao Liao[#], Yuan-Kai Shih[#], Guo-Wei Huang[*], Yu-Shao Shiao[*]

[#] *Department of Electrical Engineering, National Taiwan University of Science and Technology*
No. 43, Sec 4., Keelung Rd., Taipei 10607, Taiwan (R.O.C.)

[*]*National Nano Device Laboratories*
No.26, Prosperity Road I, Hsinchu Science Park, Hsinchu, 30078, Taiwan (R.O.C.)

[1] *m10007622@mail.ntust.edu.tw*

***Abstract*—Advances in solid state technology have helped realizing wireless communications using millimeter waves and so does the need for antenna measurement in this band. This paper reviewed several antenna measurement range designs. Their pros and cons are studied. A measurement apparatus, which is crafted to co-work with large, heavy mixer modules of an E-band network analyzer, was proposed. The measurement range contains a 2D scanner, which takes samples on a planar surface in the farfield. Collected data can be transformed to provide antennas' farfield patterns. Preliminary experiments were taken in the X-band to verify the effectiveness of the proposed measurement configuration.**

I. INTRODUCTION

The millimeter wave (mmWave) band is defined between 30 to 300 GHz. Corresponding wavelengths ranges from 10 and 1 millimeter. Because of mmWave is much smaller than microwave in terms of wavelength, Radio frequency (RF) circuit elements can be miniaturized and integrated into communication chips. Furthermore, the antenna component, which is in the range of a few millimetres, can also be integrated to the enclosure of the mmWave RFIC package.

Current mmWave band applications can be grouped into two categories, which are wireless communications and radar related uses. Due to the short wavelength, large propagation loss is unavoidable. Most applications are aimed to uses on short distance transmission [1]. As a result, mmWave wireless communication protocols can be secure and the frequency bands can be reused in different places. The other important application, which has a large market potential, is the collision avoidance radar system (CAR), which operates around the 77 GHz band. Also, security check systems based on mmWave have been implemented in airport to perform security inspection. It avoids damages caused by imaging systems based on ionizing radiations. Besides, mmWave uses on medical applications are also in development.

In principle, antennas with high directivities are required for transmitting mmWave due to large propagation attenuations. As a consequence, a transmitting antenna should be pointed to the receiving antenna precisely to secure a point-to-point link. High directivities can be realized by antenna arrays. However, antenna pattern and radiation efficiency measurements in the mmWave band have not been standardized yet due to varying characteristics in antenna feeding schemes and instrument configurations.

In theory, the conventional anechoic chamber configuration can be used to measure mmWave antennas. Nevertheless, the losses of flexible coaxial cables are too large is this band and the operation frequency of most available PNAs is not high enough. When measurements above E-band are needed, an extension module, which includes two mixers and a controller, can be installed on existing PNA systems to move the operation frequency to a higher band. Taking into consideration that the distance between antenna-under-test (AUT) and the mixer is short, and the mixer module is large and heavy, this system can't be applied to conventional anechoic chamber directly. Hence, an assessment apparatus that considers aforementioned instrumental properties is needed to evaluate radiation features of mmWave antennas.

Different types of antenna pattern measurement systems have been developed for mmWave band antennas. Table II compares the pros and cons of four different measurement systems. The measurement apparatus proposed in [2], which has a probe arm, and the one with two spinning turners [3] can provide detailed farfield patterns instantly. However, the revolving stage control system is complicated and their configurations can't accommodate large mixer modules. The range proposed in [4] can be implemented with a rather simple control system. The antenna measurement time is short. Nevertheless, it needs a signal processing algorithm to acquire the farfield pattern. On the other hand, the compact range proposed in [5] can be combined with the mixer easily and results are measured quickly. However, the compact range requires a large space and only 2D patterns are available.

II. PROPOSED MMWAVE ANTENNA MEASUREMENT RANGE

The antenna stands of the proposed 2D scanner are connected to mixer modules in a straight forward manner. The reference antenna is placed on the scanning stage along with the mixer and is facing toward the stationary AUT. The scanning stage moves horizontally and vertically to take samples on a planar surface. Note because the distances between AUT to points on the scanned plane are different, measured results can't form the farfield pattern directly. In order to acquire the desired pattern, a set of calibration

measurements and signal processing procedures should be applied to the AUT measurement results.

Fig. 1 shows the flow chart of field sampling and signal processing procedure. The first half involves measurement in a planer nearfield range installed in NTUST. The purpose is to take field samples on a planar surface in front of the AUT. The second half of the procedure transforms samples from a planer to a spherical surface. The transformed results form a distribution that is equivalent to the AUT's 3D farfield pattern. Note during measurement, the distance between the ANT and the scanner probe is kept in the farfield range to minimize the coupling between the two antennas.

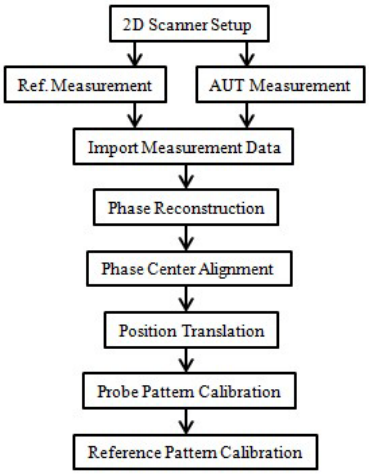

Fig. 1. Measurement procedure of the proposed 2D planner scanning range.

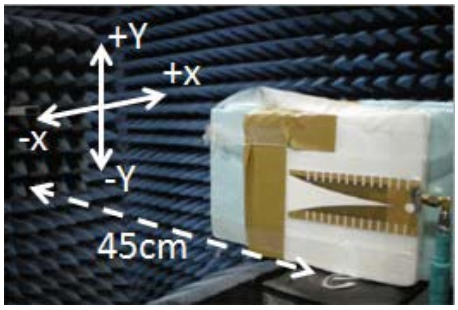

Fig. 2. Vivaldi antenna and reference probe placed in the 2D planner scanning measurement range.

This preliminary test chose a broadband Vivaldi antenna as the AUT. The Vivaldi antenna is set on the stationary stand in the range as shown in Fig. 2. It has a moderate directivity. At 12 GHz, the Vivaldi antenna's gain is about 14 dBi. A WR75 waveguide is also measured in the range to serve the reference antenna. Since the farfield pattern of the WR75 waveguide probe is known, its processed results are used to calibrate the AUT results. To the left of the picture is a WR90 waveguide, which serves as the sampling probe. It is mounted on the scanning stage. The planar surface scanned is defined as the *xy*-plane. Scanning ranges in *x*- and *y*-axes are both from -45 cm to +45 cm. For both waveguides, the lowest cut-off frequencies are greater than 8 GHz. Hence, the measurement band is chosen as the 8 to 12 GHz band, which falls into the X-band range.

III. Antenna Radiation Pattern Derivation

A. Phase Reconstruction

For the proposed antenna measurement range, several requirements should be met during sampling process to provide the desired pattern. When placed in the stage center, the sampling probe should be aligned with the AUT. The distance between phase centers of the two antennas, which is used in transforming sampled data, is supposed to be known. Under ideal circumstances, phases of sampled data should exhibit concentric patterns as shown in Fig. 3. Fig. 4 shows magnitude and phase variations taken from a measurement. The data were taken at 12 GHz with the Vivaldi antenna. In theory, when the two antennas are aligned perfectly and the estimated phase center separation distance is correct, subtracting the phase pattern in Fig. 3 from the one in Fig. 4 should yield a constant phase difference everywhere. In fact, because the antennas were set up and aligned manually, the subtraction usually produces an inhomogeneous phase difference pattern.

In order to conduct this process, sampled phases, which span from -180 to 180 degrees in the original data, are reconstructed to form a continuous, parabolic pattern as shown in Fig. 5(a). The reconstruction process begins from the center position and expands to the circumferences of the sampled plane. The phase difference from the center to the corner is about 5000 degrees. Fig. 5(b) provides the subtraction results. Note the phase difference is not a constant and there are some anomalies in the corner regions. The cause can be that the AUT does not have collocated phase centers on *x*- and *y*-axis. Also, noise in the environment or in the network analyser may interfere sampled phases. The corner region, where signal strengths are particularly weak, is subjected to noise interference.

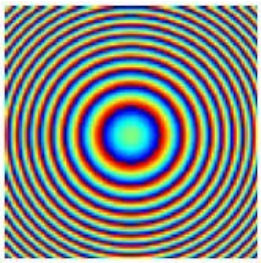

Fig. 3. Ideal phase variation on a planar surface.

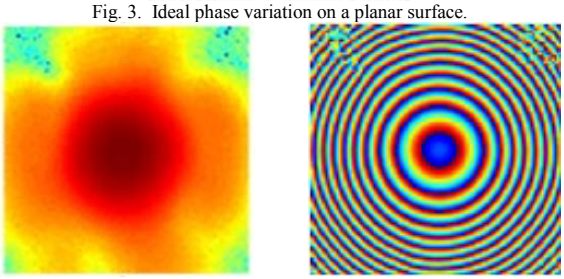

(a) Magnitude (b) Phase

Fig. 4. Measured magnitude and phase of the Vivaldi antenna at 12 GHz.

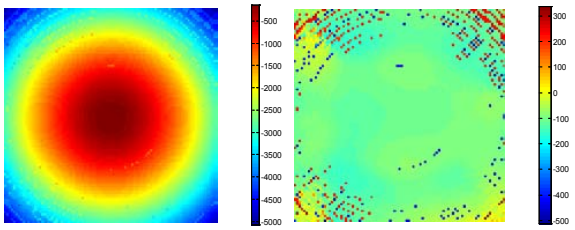

(a) Reconstucted phase (b) Calibrated phase

Fig. 5. Reconstructed and calibrated phase distributions of the Vivaldi antenna at 12 GHz.

B. *Phase Center Alignment*

The AUT phase center position and its alignment to the center of the scanning plane are critical to the farfield pattern formulation. However, above two conditions may not be met during measurements since the antennas are mounted on stands manually and the actual phase center of AUT may be unknown. Hence, before translate the sampled results to a spherical surface, we need to make sure that the phase center alignment and center separation distance are correctly estimated. Their effects on sampled results should be mitigated.

Parametric studies were conducted to assess effects of the phase center error on reconstructed phase pattern. AUT phase center alignment parameters are: x-axial offset x_0, y-axial offset y_0, and longitudinal offset L_0. The sampling step sizes in x- and y-axes are x_s and y_s respectively. Using the trial and error approach, minimum phase variations on x- and y-plane cuts were found. Calibrated patterns were shown in Fig. 6. Corresponding x_0 and y_0 values are -1 cm and 0.25 cm, respectively. If x- and y-axis offsets are incorrect, the calibrated phase variation leans on one side as seen in Fig. 7 and so does to the y-axial result.

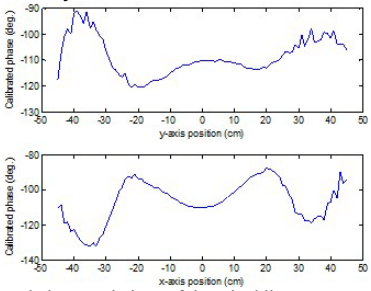

Fig. 6. Calibrated phase variations of the Vivaldi antenna on x- and y-axes. (x_o = -1 cm, y_o = 0.25 cm, L_o = -2.8 cm, x_s = 1.02 cm, y_s = 0.995 cm)

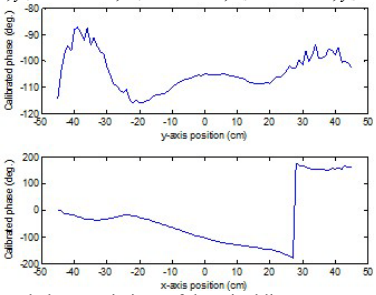

Fig. 7. Calibrated phase variations of the Vivaldi antenna on x- and y-axes. (x_o = -2 cm, y_o = 0.25 cm, L_o = -2.8 cm, x_s = 1.02 cm, y_s = 0.995 cm)

Longitudinal offset tuning is also crucial. In our measurements, the AUT phase center was initially assumed to be 6.1 cm away from the ends of the horn opening and the distance to the sampling probe is 45 cm. Fig. 8(a) shows calibrated x- and y-plane phase variations, which exhibit concave down patterns. Comparing to Fig. 6 results, this indicates the assumed phase center is too far away from the sampling waveguide when L_0 is chosen as +1 cm. On the contrary, when L_0 is set to -5 cm, calibrated patterns shown in Fig. 8(b) becomes concave up. As a result, phase center positions of a broadband antenna, which usually moves as the operation frequency changes, can be estimated with this phase reconstruction process.

Although the nearfield scanner is driven by precise stepping motors, it still may accumulate some positioning errors during measurements. The sampling spacings on x- and y-axes are assumed to be 1 cm. Fig. 9 show corrected x_s and y_s step sizes, which are 1.05 and 0.985 cm, respectively.

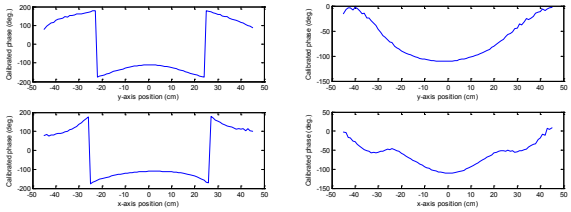

(a) L_o = 1 cm (b) L_o = -5 cm

Fig. 8. Effects of longitudinal offset on calibrated x- and y-axes phases of Vivaldi antenna. (x_o = -1 cm, y_o = 0.25 cm, x_s = 1.02 cm, y_s = 0.995 cm)

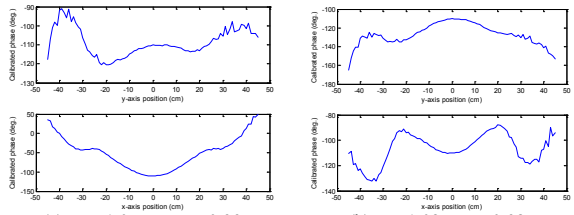

(a) x_s = 1.05 cm, y_s =0.995 (b) x_s =1.02, y_s = 0.985 cm

Fig. 9. Effects of x- and y-axes step sizes on calibrated x- and y-axes phases of Vivaldi antenna. (x_o = -1 cm, y_o = 0.25 cm, L_o = -5 cm)

C. *Position Translation*

Position translation can be executed once the sampled phases are reconstructed and calibrated. Using (1), we can translate the sampled electric field from a planar surface to a spherical one. $E_{pl}(\theta,\phi)$ represents sampled electric fields on the sampled plane; L is the shortest distance from AUT to the sampled plane; $R(\theta,\phi)$ is as the distance between the sampled point to AUT phase center.

$$E_{sp}(\theta,\phi) = E_{p\ell}(\theta,\phi)\frac{R(\theta,\phi)}{L}e^{-j\beta(L-R(\theta,\phi))} \quad (1)$$

Equation (2) is used to transfer measured E-field from rectangular coordinates to the spherical coordinate system.

$$\begin{bmatrix} E_x \\ E_y \\ E_z \end{bmatrix} = \begin{bmatrix} \sin\theta\cos\phi & \cos\theta\cos\phi & \sin\phi \\ \sin\theta\sin\phi & \cos\theta\sin\phi & \cos\phi \\ \cos\theta & -\sin\theta & 0 \end{bmatrix} \begin{bmatrix} E_r \\ E_\theta \\ E_\phi \end{bmatrix} \quad (2)$$

E_r term can be ignored in (3) and (4) since the antenna separation distance satisfies the farfield condition.

$$E_y = E_\theta \cos\theta \sin\phi + E_\phi \cos\phi \quad (3)$$

$$E_z = -E_\theta \sin\theta \quad (4)$$

At the broadside direction (θ=90°, ϕ=0°), E_y is mainly made of the $E_\phi\cos\phi$ term due to the small ϕ value. As the ϕ angle increases, $E_\theta\cos\theta\sin\phi$ increases as well and can be regarded as a supplementary term. On the other hand, E_ϕ component does not contribute to the E_z term. When θ equals to 90 degrees, E_z equals to the E_θ term.

Using (3) and (4), the needed E_ϕ and E_θ terms can be derived from measured E_z and E_y as specified in (5) and (6).

$$E_\theta = -\frac{E_z}{\sin\theta} \quad (5)$$

$$E_\phi = \frac{1}{\cos\phi}\left(E_y - \tan\theta \sin\phi E_z\right) \quad (6)$$

In this preliminary measurement, only vertically polarized term E_z was acquired. Use (5), the E_θ pattern can be derived without errors. On the contrary, the E_ϕ pattern can't be constructed completely without horizontally polarized E_y samples. As the ϕ angle increases, the importance of the E_z term elevates.

The result shown in Fig. 10 includes both the WR90 waveguide and the AUT patterns since the sampling probe doesn't aim at AUT at all times. In order to remove the sampling probe pattern, the processed pattern of AUT is subtracted from the processed reference antenna pattern, which is the WR75 waveguide. The final step is to calibrate the reference antenna pattern using the known WR75 waveguide pattern. Fig. 11(a) shows the processed Vivaldi antenna gain pattern near the main beam direction. Fig. 11(b) compares the simulated and measured patterns on the H-plane. The two curves are in good agreement.

IV. Conclusion

In this work, we demonstrated that the proposed scanning range is capable of providing AUT farfield patterns based on field samples taken on a planer surface using the developed signal processing procedure. Comparing with other mmWave ranges, the proposed range configuration is simple in terms of the scanner structure and the control method. The proposed scanner is compatible with those large mixer modules used for E-band measurements and beyond. Furthermore, phase center alignment is not critical during measurement since the center position can be determined in the signal processing stage. This feature is particularly useful for broadband antenna. As to the short comings of the proposed scanner, the primary limit is that the range can only provide part of the 3D pattern in one measurement. To cover a broader area, several of measurements should be taken and their results have to be stitched together in the post processing stage. This can be a time consuming job. As to future works, the proposed scanner range is scheduled to be implemented in the E-band with mixer modules in place. Also, the signal processing algorithms can be optimized to find the phase center automatically.

One can expect that in the near future, the need for mmWave antenna pattern assessment will grow rapidly. The development of an appropriate measurement range is a must. The proposed 2D scanning range, which has several advantages, including low fixture cost, simple control process, 3D pattern, and moderate measurement time, is helpful in evaluating the characteristics of mmWave antennas, which are critical to the development of advanced radar systems and wireless communications in this band.

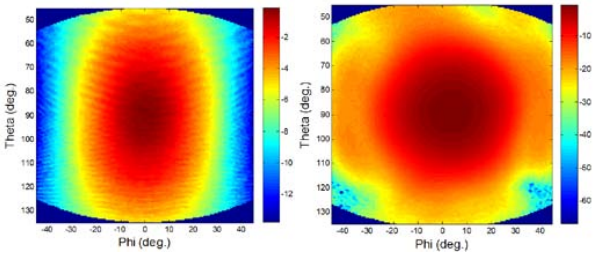

(a) WR-75 waveguide (b) Vivaldi antenna

Fig.10. Translated E_θ patterns of reference and AUT antennas

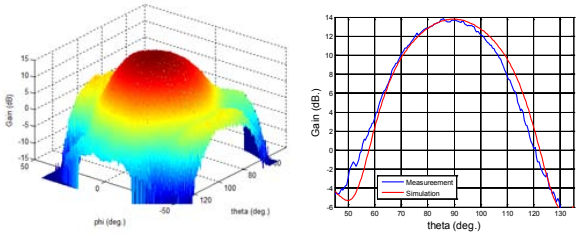

(a) 3D pattern (b) H-plane pattern

Fig.11. Calibrated 3D and H-plane AUT patterns.

References

[1] High Frequency Electronics, "A growing number of applications boosts mm-Wave technology," *High Frequency Electronics*, vol.5, no. 5, May 2006.

[2] J. A. G. Akkermans, R. van Dijk, and M. H. A. J. Herben, "Millimeter-wave antenna measurement," in *Proceedings of the 37th European Microwave Conference*, pp.83-86, 2007.

[3] S. Ranvier, M. Kyro, C. Icheln, C. Luxey, R. Staraj, and P. Vainikainen, "Compact 3-D on-wafer radiation pattern measurement system for 60 GHz antennas," *Microwave and Optical Technology Letters*, vol. 51, no. 2, pp. 319-324, 2009.

[4] T. Brockett and Y. Rahmat-Samii, "A bipolar near-field measurement system for compact millimeter-wave antenna arrays," *in Proceedings of 2010 IEEE International Symposium on phased Array Systems and Technology (ARRAY)*, pp. 292-297, Oct. 2010.

[5] S. L. Smith, J. W. Aecher, G. P. Timms, K. W. Smart, S. J. Barker, S. G. Hay, and C. Granet, "A millimeter-wave antenna amplitude and phase measurement system," *IEEE Trans. Ant. Propag.*, vol. 60, no. 4, pp. 1744-1757, Apr. 2012.